Proceedings of the Canadian Society for Mechanical Engineering International Congress
32nd Annual Conference of the Computational Fluid Dynamics Society of Canada
Canadian Society of Rheology Symposium
CSME-CFDSC-CSR 2025
May 25–28, 2025, Montréal, Québec, Canada

Multi-Stage Topology Optimization of Electric Motor for Urban Air Mobility Vehicle

Yuhao Huang[1], Shayan Jalayer[1], Hansu Kim[1], Jaesung Huh[2], Il Yong Kim[1*]
[1]Department of Mechanical and Materials Engineering, Queen's University, Kingston, Canada
[2]Korea Aerospace Research Institute, Daejeon, South Korea
*kimiy@queensu.ca

Abstract—This paper presents the conceptual design optimization of the shaft and stator for a permanent magnet synchronous motor (PMSM) used in electric vertical take-off and landing (eVTOL) vehicles. A multi-stage topology optimization (TO) and design of experiments (DOE) approach minimizes component mass while satisfying structural and performance constraints. The results demonstrate an effective framework for lightweight motor design tailored to the unique challenges of urban air mobility (UAM).

Keywords- Topology Optimization; Design of Experiment; Electric Motor; Urban Air Mobility;

I. INTRODUCTION

Urban air mobility is a growing field in transportation, with significant public and private investments for its research and development. Similarly, there is a shift from internal combustion engines to battery electric propulsion across all fields of transportation, driven by the need to reduce carbon emissions. While the limited energy density of batteries has historically hindered the feasibility of electric propulsion for aircraft, advancements in battery technology have opened new possibilities. Recent improvements in lithium-ion batteries have significantly increased their energy density compared to earlier generations. Furthermore, emerging technologies, such as solid-state, lithium-sulfur, and lithium-air batteries, are projected to achieve energy densities exceeding 500 Wh/kg within the next decade [1, 2].

With these advancements, the design of lightweight electric motors is critical for improving energy efficiency, extending flight range, and enhancing maneuverability in electric aircraft. This work focuses on the conceptual design optimization of the shaft and stator for a permanent magnet synchronous motor (PMSM), a critical component of the electric propulsion system for electric vertical take-off and landing (eVTOL) urban air mobility (UAM) vehicles. The design methodology incorporates a multi-stage topology optimization (TO) process to generate lightweight and stiff structures, alongside a design of experiments (DOE) approach to refine key geometric parameters to minimize the mass while meeting performance requirements. TO has been used extensively in automotive [3] and aerospace [4, 5] design to effectively create high-performance and lightweight structures.

The goal of this study is to minimize the mass of the PMSM shaft and stator while satisfying constraints on displacement, stress, and natural frequency. The combined use of TO and DOE provides an effective framework for designing lightweight and efficient motor components, addressing the unique challenges of UAM applications.

II. PROBLEM DEFINITION

The design framework presented in this paper is motivated by the challenge of designing a lightweight stator and shaft for an electric PMSM for an eVTOL UAM. The objective of this design is to minimize the mass of the two components, while satisfying constraints on displacement, stress, and natural frequency. This section defines the PMSM's geometry and design variables, loadcases, candidate materials, modelling assumptions, and finally the design objective and requirements.

A. Geometry & Design Variables

The motor assembly consists of a shaft and stator, which are connected by two angular contact bearings. The shaft has two sections – the shaft tube and the shaft head, which includes 12 bolt holes. The stator has eight bolt holes, and is surrounded by a cooler that's design is outside the scope of this work.

The design space for TO consists of the shaft head and the stator, while the topology of the shaft tube and a thin cooler surrounding the stator are not designable. The four design variables for size optimization by DOE are the inner radius of the shaft tube, R_1, the outer radius of the shaft tube, R_2, the inner radius of the stator, R_3, and the outer radius of the shaft head, R_4. The design space for TO and design variables for DOE are labeled and shown in the cross-sectional diagram of the motor assembly in Fig. 1.

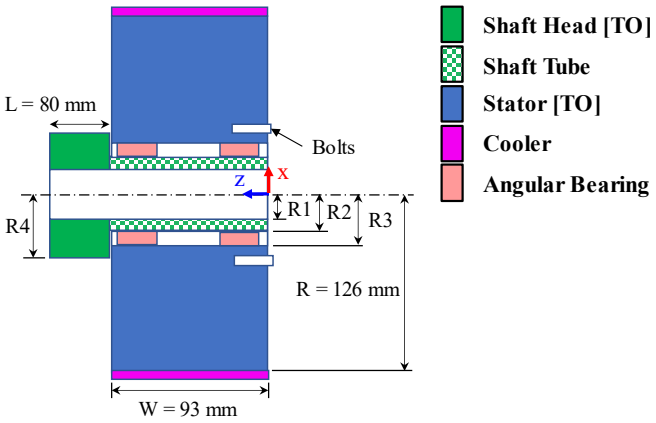

Figure 1. Cross-sectional diagram of motor assembly, showing the design variables and some outer dimensions.

B. Load Cases

There are eight static structural load cases representing reaction forces from the propeller, attached to the shaft head, four different mission stages, each for two different configurations of propulsion systems: lift and tilt. Boundary conditions are located at the eight bolt holes on the stator, shown by two blue triangles in Fig 2, where only two bolts are visible in this cross-sectional view. Multi-axial forces and moments for all load cases are applied to 12 bolt holes at the surface of the shaft head, where the motor would attach to a propeller. The moment about the Z axis, M_z, is applied to the outer surface of the cooler, where coil windings would be located.

Due to the proprietary nature of the information, specific details for the forces and moments are approximated and altered for publication. The forces in X and Y direction are in the hundreds of newtons, the forces in Z direction are in the thousands of newtons, and the moments are in the hundreds of newton-meters. Table I shows the approximate loads of 8 load cases, for reference.

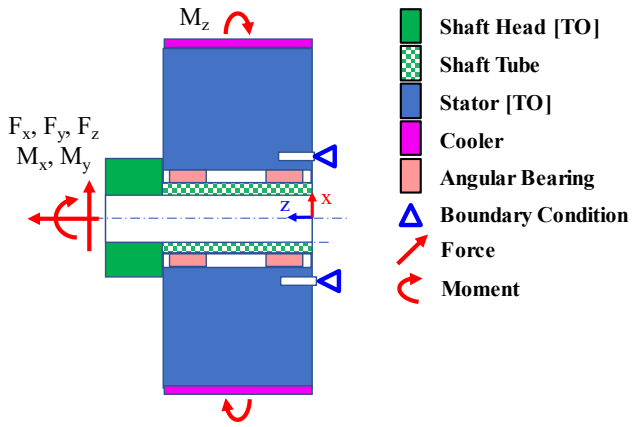

Figure 2. Cross-sectional diagram of motor assembly, showing boundary conditions and load application locations

TABLE I. LOADCASES WITH APPROXIMATE FORCE AND MOMENT COMPONENTS

#	F_x [N]	F_y [N]	F_z [N]	M_x [Nm]	M_y [Nm]	M_z [Nm]	Load Case
1	0	0	4000	0	0	-600	Take-off [Tilt]
2	0	0	4000	0	0	-400	Take-off [Lift]
3	100	-40	3000	400	400	-400	Transition [Tilt]
4	100	-400	4000	400	400	-400	Transition [Lift]
5	40	5	1000	40	5	-400	Cruise [Tilt]
6	100	-400	2000	400	400	-100	Cruise [Lift]
7	1000	500	7000	400	500	400	OEI Take-off [Tilt]
8	1100	400	7000	500	1100	-400	OEI Take-off [Lift]

C. Materials

This problem requires the choice of material for shaft and stator. However, the reasoning for the material selection is out of scope for the methodology presented in this work. All material candidates are aerospace-grade metal alloys with similar specific stiffness. Material selection occurs after the multi-stage TO and before the DOE. During the multi-stage TO, both the shaft and stator are modeled using steel (SAE 4130) properties. For the DOE, the shaft is modeled with a titanium alloy (Ti-6AL-4V) and the stator is modeled with a magnesium alloy (Elektron-43). The relevant mechanical material properties for the alloys of steel, titanium, and magnesium are shown in Table I, and are taken from the Metallic Materials Properties Development and Standardization (MMPDS) handbook [6].

D. Finite Element Modelling

The analysis of the motor assembly is done in finite element analysis (FEA), using Altair OptiStruct. This requires some modelling assumptions to apply loads and boundary conditions, and to represent the angular contact bearing. The loads and boundary conditions are applied to rigid elements that distribute their effect over many nodes. At the shaft head, the forces and moments are distributed to 12 bolt holes. On the stator, boundary conditions are individually applied to 8 bolt holes. One-dimensional rigid elements (RBE3) are used to distribute the loads and boundary conditions to all nodes inside each of the bolt holes.

For the angular contact bearing, the inner and outer race are modeled with solid elements, sharing nodes with the shaft tube and stator design space, respectively. A rigid element (RBE2) is created for the outer surface of the inner race and another one for the inner surface of the outer race. These two rigid elements are connected using a bushing element (CBUSH), which links all translational and rotational degrees of freedom except for rotation about the Z axis.

TABLE II. MATERIAL PROPERTIES

Property	Units	Elektron-43 (Magnesium)	Ti-6Al-4V (Titanium)	SAE 4130 (Steel)
Tensile Modulus	GPa	44.8	110.3	200.0
Poisson's Ratio	-	0.35	0.31	0.32
Density	g/cm^3	1.82	4.43	7.83
Tensile Yield Strength	MPa	248	896	517

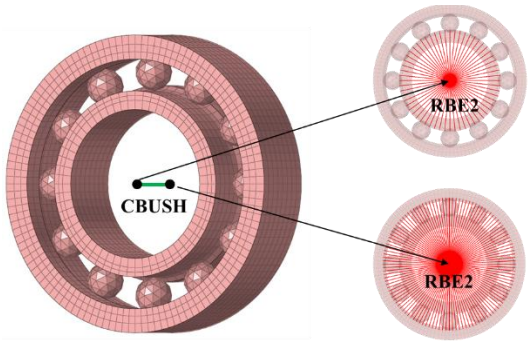

Figure 3. Angular contact bearing model, showing two rigid elements (RBE2) connecting the inner and outer race to a bushing element (CBUSH)

While an angular ball bearing allows nearly free rotation of the inner race with respect to the outer race, the bushing model uses a trivially low, non-zero torsional stiffness to avoid singularity in the solution of the FEA. The two rigid elements and one bushing element are used for each of the two bearings and are shown graphically in Fig. 3. The balls in this figure are for visualization purposes only and do not contribute to the structural performance of the model.

E. Design Requirements

Displacement, stress, and natural frequency constraints are defined for this design problem, and the overall objective is to minimize mass. The displacement is limited to 2.0 mm at the face of shaft head, where loads are applied. The stress limit is the yield strength of the materials, given in Table II, evaluated using the von Mises (VM) stress criterion. The motor components' first natural frequency must be greater than 30 Hz.

III. Design Methodology

The conceptual design optimization problem is addressed using multi-stage TO and DOE. The multi-stage TO used in this methodology has evolving constraints from stage to stage. Engineering judgement is used to assess the results from each stage and update the constraints for the following stage. The DOE uses a 2-level fractional factorial design to optimize four radius dimensions. The methodology and results for multi-stage TO and DOE are presented in this section.

A. Multi-Stage Topology Optimization

For this conceptual design, three stages of topology optimization were used. In all stages, TO is performed, and the type of problem statement is the same – minimizing compliance subject to a mass fraction constraint. This problem statement is shown mathematically in (1).

$$\begin{aligned} &\text{minimize:} && J\left(\underset{\sim}{\rho}\right) = C\left(\underset{\sim}{\rho}\right) = \sum_e \frac{1}{2} \underset{\sim}{u}^T \underset{\sim}{K} \underset{\sim}{u} \\ &\text{subject to:} && \underset{\sim}{K}\underset{\sim}{u} = \underset{\sim}{f} \\ & && g\left(\underset{\sim}{\rho}\right) = \frac{M\left(\underset{\sim}{\rho}\right)}{M_0} \le \bar{M} \\ & && \forall \text{ elements } e, \rho_e \in (0,1] \end{aligned} \tag{1}$$

Here, the objective function, J, is compliance, C. The governing equation for linear static structural analysis includes stiffness matrix, $\underset{\sim}{K}$, nodal displacement vector, $\underset{\sim}{u}$, and nodal force vector, $\underset{\sim}{f}$. For the constraint function, g, the mass of the current design, M, is divided by the mass of a fully-solid design space, M_0, and this ratio must be less than or equal to the maximum mass fraction, $\bar{M}$. In TO, for every element, e, the design variable, ρ_e, represents material existence.

While the design objective is to minimize mass, compliance minimization is used in the TO phase of the design optimization due to the limited displacement constraints available. With only one location where a displacement requirement is assessed – the face of the shaft head – a mass minimization problem would not stiffen the load paths for the torsional moment, applied to the outside of the stator, about Z axis. Instead, the compliance minimization problem creates an overall stiff structure while considering all load paths.

As mentioned, steel material properties are used for all stages of the TO. The mass fraction is calculated using the mass of an entirely solid steel design space as the value for M_0. For the shaft head, this mass is 3.9 kg, and for the stator, this mass is 32.7 kg. The mass fraction constraints are applied separately for each of the two components, to ensure meaningful results in each. For non-design components in TO, the cooler mass is 5.7 kg, the two bearings are 0.35 kg each, and the shaft tube has a mass of 0.74 kg. The final mass values reported in this section include only the mass of the design space and the shaft tube.

The finite element model used for TO is shown in Fig. 4, without one-dimensional elements shown. Note that balls in the bearings are only for visualization.

The stator, cooler, and shaft are meshed with approximately 360,000 hexahedral elements; 300,000 of which are designable, while the rest are non-designable. The non-designable regions comprise the cooler, bearing, and shaft tube.

The difference between the three stages of TO are the mass fraction, manufacturing, and symmetry constraints. The changes are determined from observations of the results in the previous stage, and the modifications aim to learn more about the design and improve the quality and practicality of the design as the design process progresses. The constraints of each stage are summarized in Table III, but were not determined a priori.

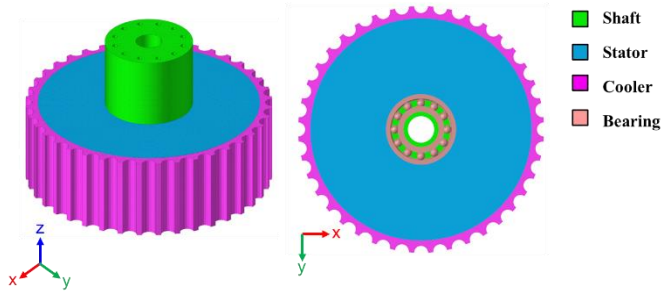

Figure 4. Isometric (a) and bottom (b) views of the finite element model.

TABLE III. CONSTRAINTS FOR MULTI-STAGE TOPOLOGY OPTIMIZATION

Stage	Mass Fraction		Symmetry	Manufacturing
	Shaft	*Stator*		
1	30%	15%	4-way mirror	-
2	30%	30%	3- and 4-way cyclic	Extrusion
3.1	40%	30%	3- and 4-way cyclic	Extrusion
3.2	40%	15%	3- and 4-way cyclic	Extrusion + Casting

1) Topology Optimization – Stage 1

Stage 1 of the TO uses the most relaxed problem statement, with fewest constraints. The only constraints are mass fractions and 4-way mirror symmetry. The optimum design is shown in Table IV, and has a few traits that we can notice and assess.

First, in the shaft head, material surrounds the bolt holes and connects them to the shaft tube at the center. The result in this region is low quality (floating elements) due to relatively small details compared to relatively large element size. The element size for the shaft head should be reduced in the following stages.

Second, the design of the stator hub is tapered, with thinner walls near the shaft head and gets thicker towards the side of the stator with bolt holes; this volume contains the load paths from the bearings to the boundary conditions at the bolt holes on the stator.

Third, a thin disc-shaped surface farthest from the shaft head contains load paths from the cooler to the bolt holes. However, this design is impractical for motor functionality due to poor heat transfer, thermal expansion, and stability concerns.

From this stage, we learn what the optimizer prioritizes and the type of design that would be generated to minimize compliance without any manufacturing constraints beyond a symmetry constraint. Since the disk is flat and solid, 4-way mirror symmetry and n-way cyclic constraints would give similar results.

2) Topology Optimization – Stage 2

In Stage 2, the 3-way cyclic constraint and 4-way cyclic constraint are used instead of the 4-way mirror symmetry to explore more design choices. Additionally, an extrusion constraint is applied to both shaft and stator, in the Z direction. This means that vertical columns of elements have identical material existence values.

The extrusion constraint prevents thin disk formation in the stator and generates spirograph curves; three triangular shapes are created when a 3-way cyclic symmetry constraint is applied, and eight thinner triangles are created when a 4-way cyclic symmetry constraint is applied.

In Stage 1, the optimizer allocated more of the stator's material far from the shaft head, and in Stage 2 the tall extrusion path leads to inefficient material use in the stator. This issue will be addressed by reducing the extrusion height in the next stage. Regarding the shaft head, the load paths near the bolt holes are still disconnected. Therefore, a slightly higher shaft mass fraction will be used in the next stage.

TABLE IV. MULTI-STAGE TOPOLOGY OPTIMIZATION RESULTS

Stage	Isometric View	Bottom View	Metrics
1 (4-way morror symm.)		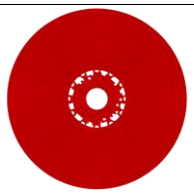	*Mass* 6.84 kg *Compliance* 3,729 mJ
2 (3-way cyclic symm.)	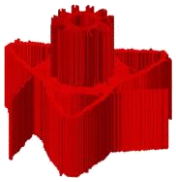		*Mass* 11.64 kg *Compliance* 4,025 mJ
2 (4-way cyclic symm.)	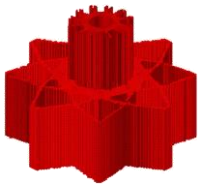		*Mass* 11.74 kg *Compliance* 4,020 mJ
3 (3-way cyclic symm.)	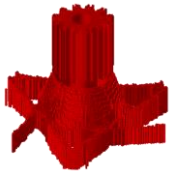		*Mass* 7.22 kg *Compliance* 3,968 mJ
3 (4-way cyclic symm.)	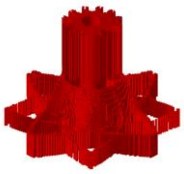	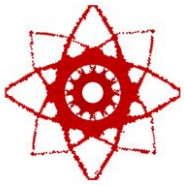	*Mass* 7.22 kg *Compliance* 3,961 mJ

3) Topology Optimization – Stage 3

Stage 3 is formulated as a two-step TO process aimed at refining the design. In the first step, the same cyclic and extrusion constraints from Stage 2 are retained, but the shaft head's mass fraction is increased to 40% to reinforce the load paths near the bolt holes. In the second step, the shaft head design is fixed, and a casting constraint is used in addition to the extrusion constraint, optimizing the stator's extrusion height while ensuring void elements remain above solid ones. The transition point is designable between the 30% and 100% of the total height, as shown in Fig. 5.

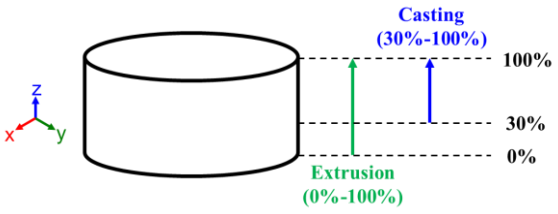

Figure 5. Diagram depicting extrusion and casting constraint bounds and directions

Stage 3 is the culmination of previous stages. The tapered hub and concentration of stator mass away from the shaft head that was noticed in Stage 1 are present in the Stage 3 results, in Table IV. From the bottom view, the Stage 2 and 3 optimum designs look nearly identical for both types of symmetry constraints. Note that Table IV omits the intermediate result, from step 1, which is very similar to the Stage 2 results, but with slightly more mass in the shaft head.

In terms of mass and compliance, the Stage 3 results are nearly identical between the jobs using 3-way and 4-way cyclic symmetry constraints. The design using 4-way cyclic symmetry constraint is selected for reinterpretation in CAD and to take into the following design phase.

B. *Design of Experiments*

Determining the optimum radii values that minimize mass while meeting design requirements often incurs significant computational costs using conventional methods. To address this challenge, a DOE approach [7] is employed. The full factorial design is one of the simplest and most straightforward methods for designing experiments. It enables the analysis of both main effects and interactions between input variables without confounding. However, evaluating every possible combination of factor levels results in high computational costs.

To overcome computational challenges, fractional factorial design provides an effective alternative for designing experiments. As a subset of the full factorial design, it offers a representative sample of the design space. Typically, the standard Yates order is used to select this subset. Fig. 6 illustrates a 2-level fractional factorial design for three input variables. Depending on the resolution, main effects and/or interactions may be confounded. For this paper, higher-order interactions are assumed to be negligible.

To reduce the number of input variables, R_3, the inner radius of the stator, is assumed to be twice the value of R_2, the outer radius of the shaft tube. For confidentiality, each design boundary is written as a function of the nominal (initial) value of each radius variable. The nominal values of each radius variable are r_1, r_2, r_3, and r_4. The adjusted design boundaries are $0.8r_1 \leq R_1 \leq 1.13r_1$, $r_2 \leq R_2 \leq 1.25r_2$, and $0.8r_4 \leq R_4 \leq 1.2r_4$. Using these modified design boundaries, a 2-level fractional factorial design with resolution III is formulated, as shown in Table V. The corresponding shaft and stator design based on this 2-level fractional design and FEA results are summarized in Tables VI and VII, respectively.

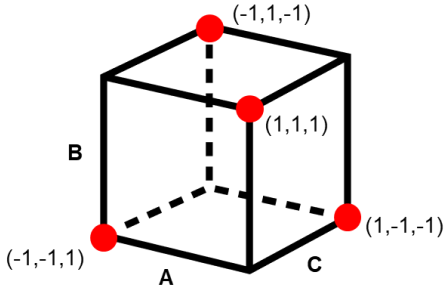

Figure 6. 2-level fractional factorial design for three input variables.

TABLE V. 2-LEVEL FRACTIONAL FACTORIAL DESIGN WITH RESOLUTION III FOR THREE DESIGN VARIABLES

Run	Size Design Variables [mm]			$R_3(=2R_2)$
	R_1	R_2	R_4	
1	$0.8r_1$ (LB)	r_2 (LB)	$1.2r_4$ (UB)	$2r_2$
2	$0.8r_1$ (LB)	$1.25r_2$ (UB)	$0.8r_4$ (LB)	$2.5r_2$
3	$1.13r_1$ (UB)	r_2 (LB)	$0.8r_4$ (LB)	$2r_2$
4	$1.13r_1$ (UB)	$1.25r_2$ (UB)	$1.2r_4$ (UB)	$2.5r_2$

LB: Lower Bound / UB: Upper Bound

TABLE VI. SHAFT AND STATOR DESIGNS BASED ON THE FRACTIONAL FRACTORIAL DESIGNS

Run	Shaft	Stator	Assembly
1		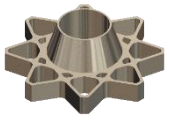	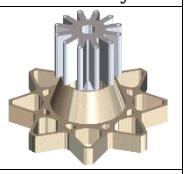
2		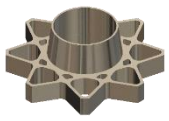	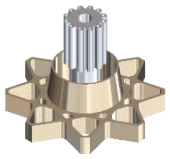
3		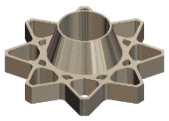	
4		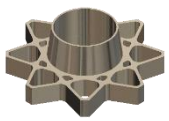	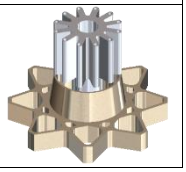

Based on the fractional factorial design and the corresponding FEA results, the main effects between input and output variables are analyzed, as illustrated in Fig. 7. In the FEA results, the maximum VM stress, in all cases, occurs during the same load case and is located on the shaft tube. The maximum VM stress values in Table VII are to be evaluated against a tensile yield strength for titanium of 898 MPa. For frequency analysis, the natural frequency at mode 2 is used, as mode 1 does not represent realistic behavior. According to the problem statement, lower values are preferred for mass, displacement, and VM stress, while higher values are desirable for frequency response.

TABLE VII. FEA RESULTS OF THE FRACTIONAL FACTORIAL DESIGNS

Run	Mass [kg]	Max. Displ. [mm]	Max. VM Stress [MPa]	Frequency [Hz]
1	3.28	0.409	263.8	959
2	2.44	0.223	131.2	966
3	2.03	0.520	447.7	959
4	3.00	0.267	167.7	966

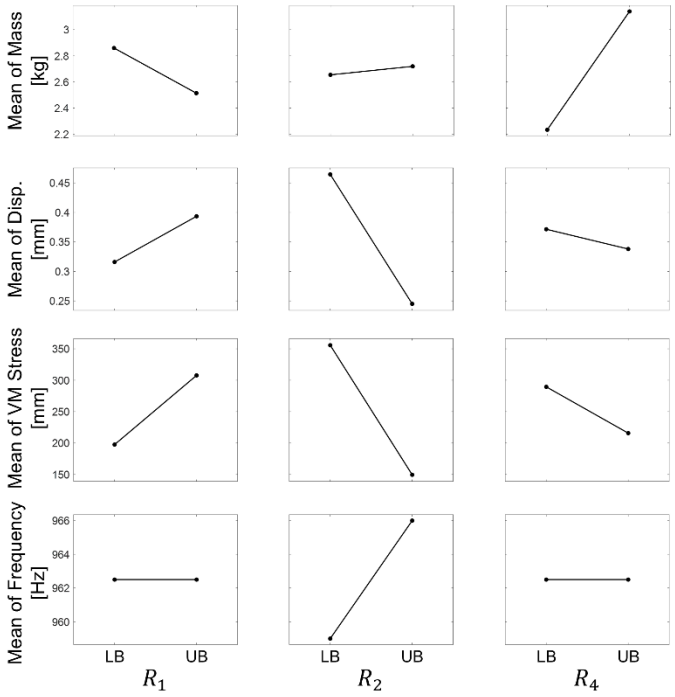

Figure 7. Main effect plots based on the fractional factorial design.

From the response characteristics, it is observed that as R_1 increases, mass decreases, but displacement and VM stress increase. For R_2 and R_4, decreasing their values reduce mas but adversely affects displacement, VM stress, and frequency response. These trends indicate a trade-off between optimizing mass and improving the other three responses. The optimum combinations of design variables for enhancing the responses are summarized in Table VIII.

According to the problem statement, the objective is to minimize the system's mass while satisfying design requirements for displacement, VM stress, and frequency. To achieve this, the optimum design is characterized by setting R_1 to its upper bound and R_2 and R_4 to their lower bounds, provided the design requirements are met. The response values for the optimum design have been analyzed in Run 3, which confirms that the design requirements are satisfied within the specified limits. The optimum design from Run 3 of the fractional factorial design is taken as the final conceptual design. Its size parameters are detailed in Tables V, the design is shown graphically in Table VI, and its performance is summarized as part of Table VII.

TABLE VIII. OPTIMUM COMBINATIONS FROM THE FRACTIONAL FACTORIAL DESIGN

Response	**Size Design Variables [mm]**		
	$\boldsymbol{R_1}$	$\boldsymbol{R_2(=0.5R_3)}$	$\boldsymbol{R_4}$
Mass	$1.13r_1$ (UB)	r_2 (LB)	$0.8r_4$ (LB)
Disp.	$0.8r_1$ (LB)	$1.25r_2$ (UB)	$1.2r_4$ (UB)
VM Stress	$0.8r_1$ (LB)	$1.25r_2$ (UB)	$1.2r_4$ (UB)
Frequency	-	$1.25r_2$ (UB)	-

This final conceptual design is lightweight – 2.03 kg for the shaft and stator, combined – and has as a factor of safety of 3.8 for displacement and 2.0 for stress, and a natural frequency 32 times greater than the minimum of 30 Hz. The safety factors are high at the end of the conceptual phase to ensure a feasible design; further lightweighting and lowering the safety factors to push the limits of efficiency should be conducted as part of the subsequent detailed design phase.

IV. CONCLUSIONS AND FUTURE WORK

A multi-stage method for TO is presented, in conjunction with a DOE study to determine a conceptual design for the shaft and stator of a PMSM, as part of an electric propulsion system for a UAM vehicle. The multi-stage TO with evolving constraints, including the creation of a custom manufacturing constraint, was successfully used to generate a stiff design with efficient use of material. DOE was then used to study the main effects of four radius values that describe the shaft and stator. This information is used to optimize the radius values in order to minimize mass without violating any design constraints.

The conceptual design is lightweight and has a safety factor of 2.0 for stress, and more for the displacement and natural frequency constraints. The safety factors are high at the end of the conceptual phase to ensure a feasible design; further lightweighting and lowering the safety factors to push the limits of efficiency are left to a subsequent detailed design phase.

While the sequential approach of doing TO first, and size optimization using DOE second was successfully used to create a conceptual design, opportunities for improvement are possible. If the topology and size optimizations are simultaneous, the combined set of design variables allows for the exploration of all possible topologies and size parameters.

REFERENCES

[1] G. Lampic, G. Gotovac, H. Geaney, and C. O'Dwyer, "Comparing the suitability of Lithium ion, Lithium Sulfur and Lithium air batteries for current and future vehicular applications," digital preprint, arXiv:1606.06347, 2016.

[2] Y.-T. Liu, S. Liu, G.-R. Li, and X.-P. Gao, "Strategy of Enhancing the Volumetric Energy Density for Lithium-Sulfur Batteries," Advanced Materials, 33(8), 2003955, 2021.

[3] C. Li and I. Y. Kim, "Topology, size, and shape optimization of an automotive cross car beam," J. Automobile Engineering, 229(10), pp. 1361-1378, 2014.

[4] O. Blair, S. Jalayer, J. Huh, S. Jun, and I. Y. Kim, "Multi-material topology optimization of an urban air mobility vehicle battery pack," AIAA SciTech Forum, January 2023.

[5] H. Kim, L. Crispo, A. Patel, N. Galley, S. M. Yeon, Y. Son, and I. Y. Kim, "Design of a metal additive manufactured aircraft seat leg using topology optimization and part decomposition," Rapid Prototyping Journal, vol. 30 no. 5, pp. 947-969, 2024.

[6] R. C. Rice, J. L. Jackson, J. Bakuckas, and S. Thompson, "Metallic Materials Properties Development and Standardization (MMPDS)," U.S. Department of Transportation, Washington, 2003.

[7] T. J. Santner, B. J. Williams, and W. I. Notz, "The Design and Analysis of Computer Experiments," New York: McGraw Hill LLC, 2014.